J. Fluid Mech. (2009), *vol.* 641, *pp.* 509–520.
doi:10.1017/S0022112009992369

Nonlinear refraction–diffraction of water waves: the complementary mild-slope equations

YARON TOLEDO AND YEHUDA AGNON†

Civil and Environmental Engineering, Technion – Israel Institute of Technology, Technion City, Haifa 32000, Israel

(Received 8 March 2009; revised 13 September 2009; accepted 20 September 2009)

A second-order nonlinear frequency-domain model extending the linear complementary mild-slope equation (CMSE) is presented. The nonlinear model uses the same streamfunction formulation as the CMSE. This allows the vertical profile assumption to accurately satisfy the kinematic bottom boundary condition in the case of nonlinear triad interactions as well as for the linear refraction–diffraction part. The result is a model with higher accuracy of wave–bottom interactions including wave–wave interaction. The model's validity is confirmed by comparison with accurate numerical models, laboratory experiments over submerged obstacles and analytical perturbation solutions for class III Bragg resonance.

Key words: Bragg resonance, coastal and offshore engineering, mild-slope equation, nonlinear waves, streamfunction formulation

1. Introduction

The irrotational flow of an incompressible homogeneous inviscid fluid is generally a three-dimensional problem. However, for practical water-wave problems, this three-dimensional formulation is usually reduced to a two-dimensional one. Among the most common types of approximated equations that allow for this reduction are the equations of the mild-slope (MS) type, which are posed in the frequency domain and are essentially linear. In these equations, a vertical structure, which relates to the horizontal bottom case, is assumed, and the problem is averaged over the depth to enable the elimination of the vertical coordinate.

One of these MS-type equations is the complementary mild-slope equation (CMSE), which was presented by Kim & Bai (2004). Its main difference is that it is derived in terms of a streamfunction vector rather than in terms of a velocity potential or the surface elevation. This enables the vertical structure to satisfy exactly the kinematic boundary condition on the uneven bottom, whereas in the case of the potential vertical structure assumption, which is used by other MS-type equations, the bottom boundary condition is only satisfied on a horizontal bottom.

For two-dimensional problems, the CMSE was shown to be in better agreement with the exact linear theory compared with other MS-type equations (Kim & Bai 2004). In the three-dimensional case, using the CMSE is essentially different, as it becomes a vector equation. For this problem to be well defined, the equation needs to be reformulated and supplemented with additional boundary conditions. These

† Email address for correspondence: agnon@tx.technion.ac.il

difficulties were accounted for, and the superior accuracy of the CMSE model was reassured in the three-dimensional case as well (Toledo 2008).

For solving nonlinear problems, Kaihatu & Kirby (1995) extended the work of Agnon *et al.* (1993) and constructed a model consisting of a set of MS equations coupled with quadratic nonlinear terms, which account for resonant triad interactions. Still, the potential formulation, which does not satisfy exactly the bottom boundary condition, was used in these nonlinear models. These equations were later used to study stochastic triad interaction (Agnon & Sheremet 1997; Eldeberky & Madsen 1999; Stiassnie & Drimer 2006).

Using Cosserat surfaces, Green & Naghdi (1976) developed an alternative approach for modelling incompressible fluid dynamic problems. Among other flow problems, it was as well applied to water waves (see, for example, Ertekin & Becker 1998). Constricting this approach for sheet-like flows, Kim *et al.* (2001) have derived the irrotational Green–Naghdi (IGN) equations. Further more, a Lagrangian description of the IGN equations specifically for water waves was written using the streamfunction formulation (Kim *et al.* 2003; Kim, Ertekin & Bai 2007).

The main objective of this work is to construct a nonlinear model using a streamfunction formulation. The nonlinear model is to consist of a set of CMSEs coupled with quadratic nonlinear terms. This model is expected to have an improved accuracy in both the linear and the nonlinear parts because of the exact satisfaction of the kinematic boundary condition on the uneven bottom.

The paper is organized as follows: in § 2 the IGN Lagrangian is presented; a superposition of solutions with a vertical profile approximation is applied in § 3; and the nonlinear CMSE model is constructed under the assumption of time-harmonic waves in § 4; finally, in § 5 the model's numerical results are compared with accurate numerical simulations, laboratory experiments and analytical perturbation solutions.

2. The irrotational Green–Naghdi Lagrangian

Define Ψ as a streamfunction vector,

$$\Psi(\boldsymbol{x}, z, t) \equiv \int_{-h}^{z} \boldsymbol{u}(x, \zeta)\, \underline{\mathrm{d}}\zeta, \quad \boldsymbol{u} = (u, v), \quad \boldsymbol{x} = (x, y), \tag{2.1}$$

where $\boldsymbol{u}$ is the horizontal velocity vector and $\boldsymbol{x}$ is the horizontal position vector. From (2.1) the velocity field is defined as

$$\boldsymbol{u} = \frac{\partial \Psi}{\partial z}, \quad w = -\nabla \cdot \Psi. \tag{2.2}$$

The equations governing the irrotational flow of an incompressible inviscid fluid with a free surface over a horizontal bottom can be constructed using the IGN equations derived from Hamilton's principle (see Kim *et al.* 2001, 2003). The Lagrangian is given by

$$\left.\begin{aligned} \boldsymbol{L} &= \int\int L \,\mathrm{d}x\,\mathrm{d}y, \\ \frac{1}{\rho} L &= \phi\,(\eta_t + \nabla\cdot\Psi + \Psi_z \cdot \nabla\eta)_{z=\eta} + \frac{1}{2}\int_{-h}^{\eta} (|\Psi_z|^2 + |\nabla\cdot\Psi|^2)\,\mathrm{d}z - \frac{1}{2} g\eta^2. \end{aligned}\right\} \tag{2.3}$$

Here $\nabla = (\partial/\partial x, \partial/\partial y)$; $h = h(\boldsymbol{x})$ is the water depth; $\eta = \eta(\boldsymbol{x}, t)$ is the surface elevation; and $\phi = \phi(\boldsymbol{x}, t)$ is a Lagrange multiplier function. The origin is on the undisturbed water level and z is positive upward.

Taking the first variation of the Lagrangian with respect to ϕ, η and Ψ gives three Euler–Lagrange equations:

$$\frac{\delta L}{\delta \Psi}: \quad \nabla(\nabla\cdot\Psi) + \Psi_{zz} = 0, \quad -h < z < \eta, \tag{2.4}$$

$$\frac{\delta L}{\delta \eta}: \quad \phi_t + \tfrac{1}{2}(\Psi_z)^2 + \tfrac{1}{2}(\nabla\cdot\Psi)^2 + g\eta = 0, \quad z = \eta, \tag{2.5}$$

$$\frac{\delta L}{\delta \phi}: \quad \eta_t + \nabla\cdot\Psi + \Psi_z\cdot\nabla\eta = 0, \quad z = \eta. \tag{2.6}$$

By using this formulation, Kim & Bai (2004) showed that the impermeable bottom boundary condition on $z = -h(x, y)$ is satisfied exactly, and the definition of Ψ can be used to construct a Dirichlet boundary condition,

$$\Psi = 0 \quad z = -h. \tag{2.7}$$

This together with lateral boundary conditions form a complete set of equations and boundary conditions that govern the irrotational flow of an incompressible inviscid fluid with a free surface. Equation (2.5) implies that ϕ, the Lagrange multiplier for the kinematic boundary condition on the free surface, is actually the velocity potential on the free surface, as shown by Kim *et al.* (2001).

3. The approximated Euler–Lagrange equations

Expanding (2.3) around $z = 0$ by use of the Taylor series up to $O((ka)^2)$ gives

$$\frac{1}{\rho}L = \phi\left(\eta_t + \nabla\cdot\Psi + \Psi_z\cdot\nabla\eta + \nabla\cdot\Psi_z\eta\right)_{z=0} + \frac{1}{2}\int_{-h}^{0}\left(|\Psi_z|^2 + \left(\nabla\cdot\Psi\right)^2\right)\mathrm{d}z + \frac{1}{2}\eta\left(|\Psi_z|^2 + \left(\nabla\cdot\Psi\right)^2\right)_{z=0} - \frac{1}{2}g\eta^2. \tag{3.1}$$

In order to eliminate the z-coordinate and construct an MS-type equation the vertical profile can be assumed to consist of a superposition of solutions:

$$\Psi(\boldsymbol{x}, z, t) = \sum_{l=1}^{N} f_l(k_l, h, z)\Psi_l(\boldsymbol{x}, t). \tag{3.2}$$

Following Kim & Bai (2004), the vertical profiles are chosen as in the linear solution of the horizontal bottom problem,

$$f_l(k_l, h, z) = \frac{\sinh(k_l(h)(z+h))}{\sinh(k_l(h)h)}, \quad \omega_l^2 = gk_l\tanh(k_l h). \tag{3.3}$$

Substituting (3.2), Lagrangian (3.1) becomes

$$\frac{1}{\rho}L = \phi\left(\eta_t + \sum_{l=1}^{N}\nabla\cdot\Psi_l + \sum_{l=1}^{N}\bar{f}_l\Psi_l\cdot\nabla\eta + \sum_{l=1}^{N}\left(\nabla\bar{f}_l\cdot\Psi_l + \bar{f}_l\nabla\cdot\Psi_l\right)\eta\right) + IntLinPart + \frac{1}{2}\sum_{l=1}^{N}\sum_{m=1}^{N}\left(\bar{f}_l\bar{f}_m\Psi_l\cdot\Psi_m + (\nabla\cdot\Psi_l)(\nabla\cdot\Psi_m)\right)\eta - \frac{1}{2}g\eta^2, \tag{3.4}$$

where

$$\bar{f}_l \equiv \left.\frac{\partial f_l(k_l,h,z)}{\partial z}\right|_{z=0}, \tag{3.5}$$

$$\begin{aligned} IntLinPart \equiv \sum_{l=1}^{N}\sum_{m=1}^{N}\Bigg(&\frac{1}{2}\bar{d}\Psi_l\cdot\Psi_m + b\,(\nabla h\cdot\Psi_l)\,\nabla\cdot\Psi_m \\ &+\frac{1}{2}c\,(\nabla h\cdot\Psi_l)\,(\nabla h\cdot\Psi_m)+\frac{1}{2}\bar{a}\,(\nabla\cdot\Psi_l)\,(\nabla\cdot\Psi_m)\Bigg). \end{aligned} \tag{3.6}$$

Where *IntLinPart* denotes the vertically integrated linear part.

Taking the first variation of Lagrangian (3.4) with respect to ϕ, η and Ψ_n for $n=1,2,\ldots,N$ yields $2N+2$ Euler–Lagrange equations:

$$\begin{aligned} \frac{\delta L}{\delta\Psi_n}: \quad &-\nabla\phi-\nabla\phi\,\bar{f}_n\eta+LinPart_n+\left(\sum_{l=1}^{N}\bar{f}_l\Psi_l\right)\bar{f}_n\eta \\ &-\sum_{l=1}^{N}\left(\nabla\left(\nabla\cdot\Psi_l\right)\eta+\left(\nabla\cdot\Psi_l\right)\nabla\eta\right)=0, \end{aligned} \tag{3.7}$$

$$\begin{aligned} \frac{\delta L}{\delta\eta}: \quad &\phi_t+\nabla\phi\sum_{l=1}^{N}\bar{f}_l\Psi_l+g\eta \\ &-\frac{1}{2}\sum_{l=1}^{N}\sum_{m=1}^{N}\left(\bar{f}_l\bar{f}_m\Psi_l\cdot\Psi_m+\left(\nabla\cdot\Psi_l\right)\left(\nabla\cdot\Psi_m\right)\right)=0, \end{aligned} \tag{3.8}$$

$$\frac{\delta L}{\delta\phi}: \quad \eta_t+\sum_{l=1}^{N}\nabla\cdot\Psi_l+\sum_{l=1}^{N}\nabla\cdot\left(\bar{f}_l\Psi\right)\eta+\sum_{l=1}^{N}\nabla\eta\cdot\left(\bar{f}_l\Psi\right)=0, \tag{3.9}$$

where

$$\begin{aligned} LinPart_n = \bar{d}\Psi_n &- \nabla\left(\bar{a}\left(\nabla\cdot\Psi_n\right)+b\left(\nabla h\cdot\Psi_n\right)\right) \\ &+b\left(\nabla\cdot\Psi_n\right)\nabla h+c\left(\nabla h\cdot\Psi_n\right)\nabla h, \end{aligned}$$

and the definitions of $\bar{a}$, b, c and $\bar{d}$ are

$$\left.\begin{aligned} \bar{a}(h)&=\int_{-h}^{0}f^2\,\mathrm{d}z, \quad b(h)=\int_{-h}^{0}f\frac{\partial f}{\partial h}\,\mathrm{d}z, \\ c(h)&=\int_{-h}^{0}\left(\frac{\partial f}{\partial h}\right)^2\mathrm{d}z, \quad \bar{d}(h)=\int_{-h}^{0}\left(\frac{\partial f}{\partial z}\right)^2\mathrm{d}z. \end{aligned}\right\} \tag{3.10}$$

As was shown in § 2, ϕ represents the velocity potential on the free surface, and therefore

$$\nabla\phi=\Psi_z|_{z=\eta}=\sum_{l=1}^{N}\bar{f}_l\Psi_l+O((ka)^2). \tag{3.11}$$

Substituting (3.11) in (3.7)–(3.9) yields

$$\frac{\delta L}{\delta\Psi_n}: \quad -\nabla\phi+LinPart_n-\sum_{l=1}^{N}\left(\nabla\left(\nabla\cdot\Psi_l\right)\eta+\left(\nabla\cdot\Psi_l\right)\nabla\eta\right)=0, \tag{3.12}$$

$$\frac{\delta L}{\delta\eta}: \quad \phi_t+g\eta+\frac{1}{2}\sum_{l=1}^{N}\sum_{m=1}^{N}\left(\bar{f}_l\bar{f}_m\Psi_l\cdot\Psi_m-\left(\nabla\cdot\Psi_l\right)\left(\nabla\cdot\Psi_m\right)\right)=0, \tag{3.13}$$

$$\frac{\delta L}{\delta \phi}: \quad \eta_t + \sum_{l=1}^{N} \nabla \cdot \Psi_l + \sum_{l=1}^{N} \nabla \cdot \left(\bar{f}_l \Psi\right) \eta + \sum_{l=1}^{N} \nabla \eta \cdot \left(\bar{f}_l \Psi_l\right) = 0. \tag{3.14}$$

4. Time-harmonic wave propagation

The first step towards a formulation solely in terms of Ψ is to eliminate η from the nonlinear parts. In order to achieve that, linear relations can be applied, and η will be defined in terms of Ψ using a linearization of the kinematic boundary condition (2.6). In contrast, $\nabla\eta$ will be constructed by taking the gradient of the linear dynamic free-surface boundary condition (2.5) together with (3.11). This allows for a low order of spatial derivatives of Ψ:

$$\eta = -\sum_{l=1}^{N} \int \nabla \cdot \Psi_l \, \mathrm{d}t + O((ka)^2), \tag{4.1}$$

$$\nabla\eta = -\frac{1}{g} \sum_{l=1}^{N} \bar{f}_l \frac{\partial \Psi_l}{\partial t} + O((ka)^2). \tag{4.2}$$

Using the linear relations (4.1) and (4.2) and (3.12)–(3.14), the dependence on the surface elevation η can be factored out to yield $2N+1$ coupled evolution equations of Ψ_n and ϕ:

$$-\nabla\phi + LinPart_n + \sum_{l=1}^{N} \sum_{m=1}^{N} \left(\nabla (\nabla \cdot \Psi_l) \int \nabla \cdot \Psi_m dt + \frac{1}{g} (\nabla \cdot \Psi_l) \bar{f}_m \frac{\partial \Psi_m}{\partial t} \right) = 0, \tag{4.3}$$

$$\begin{aligned} \phi_{tt} = g \sum_{l=1}^{N} \nabla \cdot \Psi_l - \sum_{l=1}^{N} \sum_{m=1}^{N} \left(g \nabla \cdot \left(\bar{f}_l \Psi_l\right) \int \nabla \cdot \Psi_m dt + \bar{f}_l \bar{f}_m \Psi_l \frac{\partial \Psi_m}{\partial t} \right) \\ - \frac{1}{2} \sum_{l=1}^{N} \sum_{m=1}^{N} \frac{\partial}{\partial t} \left(\bar{f}_l \bar{f}_m \Psi_l \Psi_m - (\nabla \cdot \Psi_l)(\nabla \cdot \Psi_m) \right). \end{aligned} \tag{4.4}$$

The free-surface elevation can be calculated afterwards using the relation

$$\eta_t + \sum_{l=1}^{N} \nabla \cdot \Psi_l - \sum_{l=1}^{N} \sum_{m=1}^{N} \left(\nabla \cdot \left(\bar{f}_l \Psi\right) \int \nabla \cdot \Psi_l dt + \frac{1}{g} \bar{f}_l \frac{\partial \Psi_l}{\partial t} \cdot \left(\bar{f}_m \Psi_m\right) \right) = 0 \tag{4.5}$$

In order to construct time-harmonic evolution equations, we assume Ψ_l to be of the form

$$\Psi_m(\boldsymbol{x}, t) = \psi_m(\boldsymbol{x}) \, \mathrm{e}^{-\mathrm{i}\omega_m t} + \psi_m^*(\boldsymbol{x}) \, \mathrm{e}^{\mathrm{i}\omega_m t}, \tag{4.6}$$

where $(^*)$ denotes the complex conjugate. The free-surface elevation η and the velocity potential at the free surface, ϕ, can be assumed as a superposition of time-harmonic solutions as well,

$$\eta(\boldsymbol{x}, t) = \sum_{l=1}^{N} \left(\eta_l(\boldsymbol{x}) \, \mathrm{e}^{-\mathrm{i}\omega_l t} + \eta_l^*(\boldsymbol{x}) \, \mathrm{e}^{\mathrm{i}\omega_l t} \right), \tag{4.7}$$

$$\phi(\boldsymbol{x}, t) = \sum_{l=1}^{N} \left(\phi_l(\boldsymbol{x}) \, \mathrm{e}^{-\mathrm{i}\omega_l t} + \phi_l^*(\boldsymbol{x}) \, \mathrm{e}^{\mathrm{i}\omega_l t} \right). \tag{4.8}$$

Substituting (4.6) and (4.8) into (4.3) and (4.4), eliminating ϕ and taking into account only resonant triad interaction (i.e. the nonlinear terms that have the same angular frequency as of the linear part) yield a set of evolution equation for each harmonic ψ_n:

$$\left.\begin{aligned}
&-\nabla\left(a\left(\nabla\cdot\psi_n\right)+b\left(\nabla h\cdot\psi_n\right)\right)+\left(b\nabla\cdot\psi_n+c\nabla h\cdot\psi_n\right)\nabla h-k_n(h)^2a\psi_n\\
&-\sum_{l=1}^{n-1}\left(\frac{\mathrm{i}}{\omega_{n-l}}\nabla\left(\nabla\cdot\psi_l\right)\left(\nabla\cdot\psi_{n-l}\right)-\frac{\mathrm{i}\omega_{n-l}}{g}\left(\nabla\cdot\psi_l\right)\bar{f}_{n-l}\psi_{n-l}\right)\\
&-\sum_{l=1}^{N-n}\left(\frac{\mathrm{i}}{\omega_{n+l}}\nabla\left(\nabla\cdot\psi_l^*\right)\left(\nabla\cdot\psi_{n+l}\right)-\frac{\mathrm{i}}{\omega_l}\nabla\left(\nabla\cdot\psi_{n+l}\right)\left(\nabla\cdot\psi_l^*\right)\right.\\
&\left.-\frac{\mathrm{i}\omega_{n+l}}{g}\left(\nabla\cdot\psi_l^*\right)\bar{f}_{n+l}\psi_{n+l}+\frac{\mathrm{i}\omega_l}{g}\left(\nabla\cdot\psi_{n+l}\right)\bar{f}_l\psi_l^*\right)+\nabla\phi_n^{NL}=0,\\
&\phi_n^{NL}=\frac{1}{\omega_n^2}\sum_{l=1}^{n-1}\left(\frac{\mathrm{i}g}{\omega_{n-l}}\nabla\cdot\left(\bar{f}_l\psi_l\right)\left(\nabla\cdot\psi_{n-l}\right)\right.\\
&\left.-\mathrm{i}\left(\omega_{n-l}+\frac{1}{2}\omega_n\right)\bar{f}_l\bar{f}_{n-l}\psi_l\psi_{n-l}+\mathrm{i}\omega_n\left(\nabla\cdot\psi_l\right)\left(\nabla\cdot\psi_{n-l}\right)\right)\\
&+\frac{1}{\omega_n^2}\sum_{l=1}^{N-n}\left(\frac{\mathrm{i}g}{\omega_{n+l}}\nabla\cdot\left(\bar{f}_l\psi_l^*\right)\left(\nabla\cdot\psi_{n+l}\right)-\mathrm{i}\left(\omega_{n+l}-\omega_l+\omega_n\right)\bar{f}_l\bar{f}_{n+l}\psi_l^*\psi_{n+l}\right.\\
&\left.-\frac{\mathrm{i}g}{\omega_l}\nabla\cdot\left(\bar{f}_{n+l}\psi_{n+l}\right)\nabla\cdot\psi_l^*+\mathrm{i}\omega_n\left(\nabla\cdot\psi_l^*\right)\left(\nabla\cdot\psi_{n+l}\right)\right),
\end{aligned}\right\}\tag{4.9}$$

where

$$a(h)=\int_{-h}^{0}f^2\,\mathrm{d}z-\frac{g}{\omega^2}=\frac{\coth(kh)}{2k}\left(1+\frac{2kh}{\sinh(2kh)}\right)=-\frac{gk^2}{\omega^4}CC_g,\tag{4.10}$$

$$b(h)=\int_{-h}^{0}f\frac{\partial f}{\partial h}\,\mathrm{d}z=\frac{1}{4\sinh^2(kh)}\frac{2kh\cosh(2kh)-\sinh(2kh)}{2kh+\sinh(2kh)},\tag{4.11}$$

$$\begin{aligned}c(h)&=\int_{-h}^{0}\left(\frac{\partial f}{\partial h}\right)^2\mathrm{d}z\\&=\frac{k}{12\sinh^2(kh)}\frac{-12kh+8(kh)^3+3\sinh(4kh)+12(kh)^2\sinh(2kh)}{(2kh+\sinh(2kh))^2}.\end{aligned}\tag{4.12}$$

This set of N coupled vector equations ($2N$ scalar ones) extends the CMSE vector equation of Kim & Bai (2004) with the nonlinear triad interaction terms. If needed, ϕ_n can be calculated afterwards using the relation

$$\phi_n=-\frac{g}{\omega_n^2}\nabla\cdot\psi_n+\phi_n^{NL}.\tag{4.13}$$

5. Numerical results

5.1. *Superharmonic class III Bragg resonance*

Class III Bragg resonance refers to a nonlinear wave–wave–bottom resonant triad interaction. Its resonance conditions can be satisfied by an interaction between a single wave and an undulated bottom. For the two-dimensional problem, the superharmonic resonance creates a transmitted wave with an angular frequency 2ω and a wavenumber $2k+k_b$. Here, k_b is the wavenumber of the bottom undulation, and ω and k are the

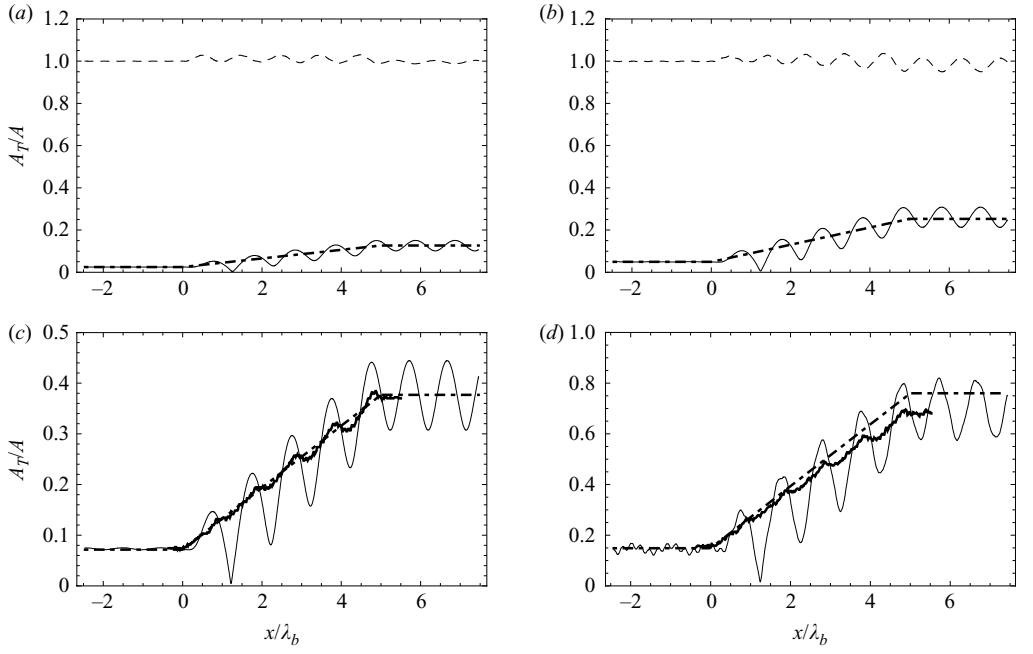

FIGURE 1. The results for class III superharmonic Bragg resonance over a patch of five sinusoidal ripples. The wave amplitude is normalized by the first-harmonic incident wave amplitude, and the position is normalized by the bottom wavelength. Panels (*a*), (*b*), (*c*) and (*d*) refer to $ka = 0.01$, 0.02, 0.03 and 0.06 respectively. The dashed line represents the first harmonic of the nonlinear CMSE model; the thin solid line represents the second harmonic of the nonlinear CMSE model including the bound wave; the thick solid line represents the second harmonic of the HOS method by Liu & Yue (1998); and the dot-dashed line represents the second harmonic of the perturbation solution by Liu & Yue (1998) accurate up to $x = O(\varepsilon^{-1})$ without the bound wave.

angular frequency and the wavenumber of the incident wave, which satisfy the linear dispersion relation, $\omega^2 = gk\tanh(kh)$.

The particular case of class III Bragg resonance over an oscillatory bottom was addressed using other models as well (Agnon, Pelinovsky & Sheremet 1998; Liu & Yue 1998; Madsen, Fuhrman & Wang 2006). Here, the bathymetry for this numerical simulation was taken as in Liu & Yue (1998): flat bottom with a patch of five sinusoidal ripples, where $k_b d = 0.025$ and $k_b h = 0.325$. The patch starts at $x = 0$ and d represents its amplitude. The solution was compared with the analytical perturbation solution and the numerical solution of Liu & Yue (1998). Note that the analytical solution is an approximation, which does not contain the bound wave, and is only accurate up to $x = O(\varepsilon^{-1})$.

Figure 1 presents the numerical results of (4.9) with two harmonics except in the case of $ka = 0.06$, which was calculated using four harmonics. The agreement with the analytical growth of the transmitted wave amplitude is excellent for lower values of ka (0.01, 0.02, 0.03). For $ka = 0.06$, we can see that towards the end of the patch the transmitted wave amplitude growth starts to decrease compared with the analytical perturbation solution. This is expected, as the analytical solution becomes less accurate at this distance. However, the initial growth of the amplitudes agree.

For $ka = 0.03, 0.06$, Liu & Yue (1998) solved this problem as well, using a high-order spectral (HOS) method. It appears that the bound wave was filtered out of their

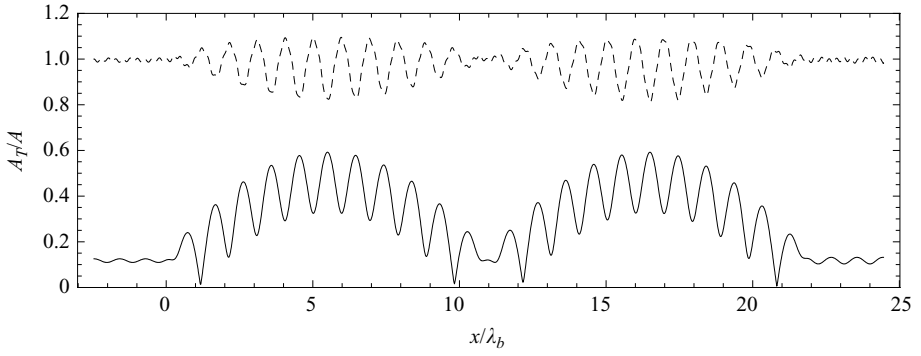

FIGURE 2. The results for the nonlinear CMSE class III Bragg superharmonic resonance over a patch of 22 sinusoidal ripples for $ka = 0.05$ and $k_b d = 0.03$. The wave amplitude is normalized by the first-harmonic incident wave amplitude, and the position is normalized by the bottom wavelength. The dashed line represents the first harmonic of the nonlinear CMSE model, and the thin solid line represents the second harmonic of the nonlinear CMSE model.

results, as their second harmonic starts with no energy, and therefore their results contain no steep undulations as the ones of the nonlinear CMSE. In figure 1, their graphs were shifted up in the magnitude of the nonlinear CMSE's bound wave to allow an easier comparison of the second-harmonic amplitude growth. Note that in any MS-type equation the bound waves are not approximated well because of the assumption of a free wave's vertical structure. Still, it is the free-wave evolution that is the most important.

The exact linearized class III condition for the above problem is $(k/k_b) = 2.031$. In the nonlinear CMSE the condition for $ka = 0.03$ was the exact one, and for $ka = 0.06$ it was 2.06. In the HOS calculations the conditions for $ka = 0.03, 0.06$ were 2.021 and 2.025 respectively. We can see very good agreement for the free-wave solution between the nonlinear CMSE and the HOS in both cases.

Mei (1985) presented a multiple-scale perturbation solution for class I Bragg resonance, where he showed that the resonant wave gains energy from the incident wave and then transfers it back in a harmonic way, as it continues to resonate on the sinusoidal patch. The same mechanism applies to the case of class III Bragg resonance; so the linear transfer of energy is expected to apply for the lower-wave-steepness (ka) calculations because the patch of five bottom wavelengths lies still within $x \leqslant O(\varepsilon^{-1})$. For higher ka or longer patches the analytical solution should apply only as the initial growth of the transmitted wave amplitude. Figure 2 presents the resulting transmitted wave amplitude for $ka = 0.05$, $k_b d = 0.03$ and a patch of 22 sinusoidal ripples, where we can see the transfer of energy back and forth.

5.2. *Submerged one-dimensional obstacle*

Beji & Battjes (1993), Dingemans (1994) and Luth, Klopman & Kitou (1980) conducted wave tank experiments of monochromatic waves propagating over a trapezoidal bar, using different scalings. The relatively shallow water together with the changes in bathymetry gives rise to near-resonant interactions, which transfer energy to higher harmonics.

The experimental set-up of Dingemans (1994) consists of a trapezoidal shoal region with an up-slope and down-slope of 1:20 and 1:10 respectively from a constant depth of $h_0 = 0.8$ m to the shallow flat bar-crest at the depth of $h_{bar} = 0.2$ m and back.

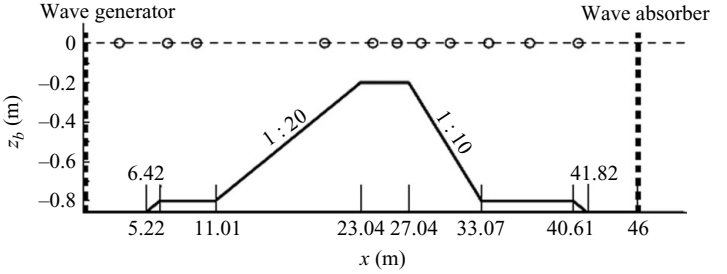

FIGURE 3. The bathymetry in the experiment of Dingemans (1994). The wavemaker is positioned at $x = 0$ with incident wave height of $H = 4$ cm and period of $T = 2.86$ s. The circles indicate the cross-sections monitored by wave gauges.

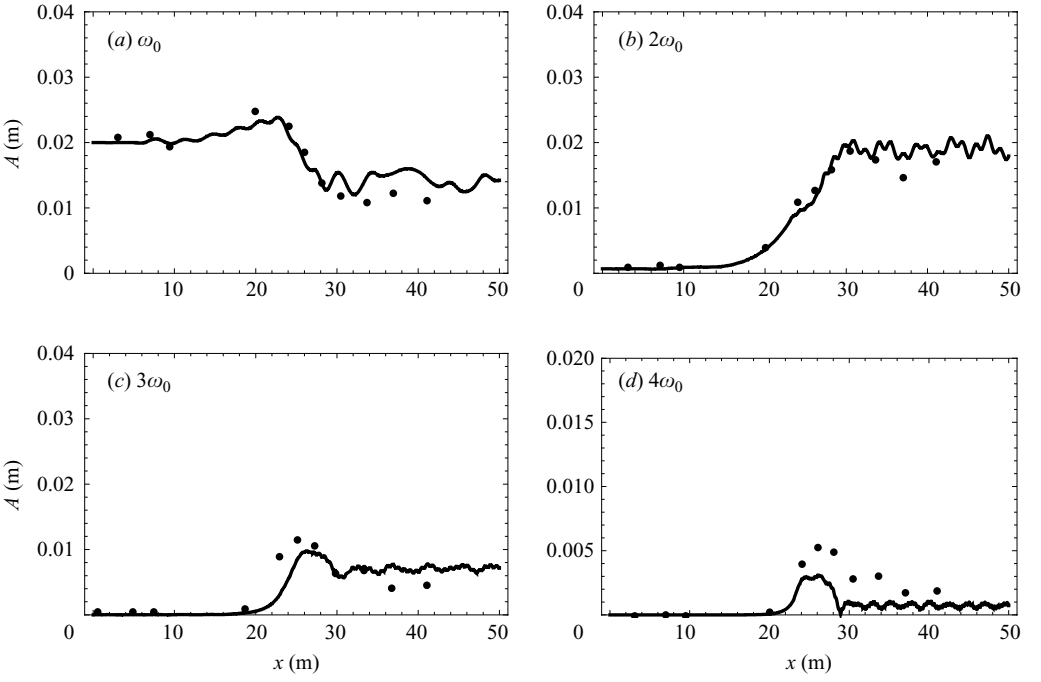

FIGURE 4. The numerical results of the nonlinear CMSE for the experiment of Dingemans (1994) (solid line) and the gauge measurements of the wave tank experiment (solid circles). Panels (*a*), (*b*), (*c*) and (*d*) show the first, second, third and fourth harmonics respectively.

The bathymetry and the monitored sections are shown in figure 3. The incident wave height was $H = 4$ cm and the period $T = 2.86$ s.

The nonlinear CMSE model (4.9) was used for the calculation taking into account four harmonics. The results for the numerical experiment together with the wave tank ones are given in figure 4. The numerical results for the first and second harmonics seem to excellently agree with the experimental results. The accuracy of the third and fourth harmonics is not expected to be high because the nonlinear part of the model is accurate up to $O((ka)^2)$. Still, the high harmonics behave qualitatively well. Quantitatively, after the shoal area, the error of the third harmonic wave is between 10 % and 20 %, and the error of the fourth is greater.

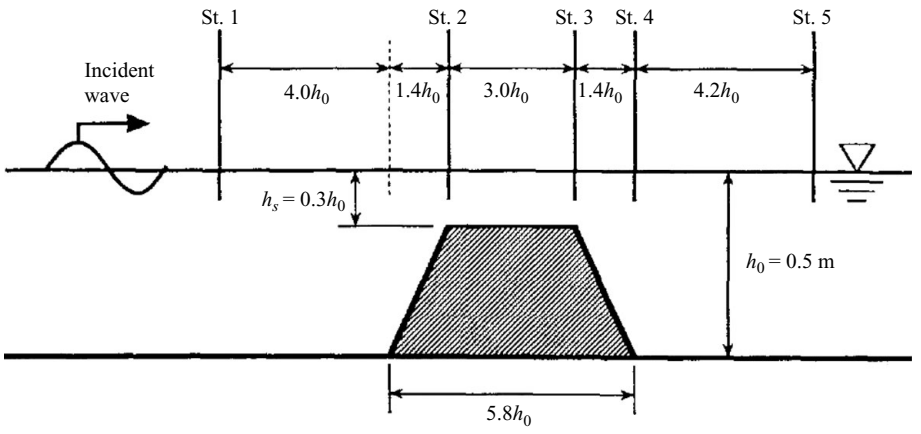

FIGURE 5. The bathymetry in the experiment of Ohyama *et al.* (1995) with incident wave height of $H = 5$ cm, period of $T = 2.682$ s and constant depth of $h_0 = 0.5$ m.

Ohyama, Kioka & Tada (1995) conducted wave tank experiments of monochromatic waves propagating towards a trapezoidal bar as well, but in their experiment the bar had steep slopes of 1:2. The main qualitative difference of this experiment is that the steep obstacle creates a significant reflected wave. The experimental set-up consists of a trapezoidal shoal region with an up-slope and a down-slope of 1:2 from a constant depth of $h_0 = 0.5$ m to the shallow flat panel at the depth of $h_{bar} = 0.15$ m. The bathymetry and the monitored cross-sections are shown in figure 5. The incident wave height was $H = 5$ cm and the period $T = 2.682$ s.

The nonlinear CMSE model (4.9) was used for the calculation, again taking into account four harmonics. The results for the numerical experiment together with the wave tank results are shown in figure 6. The numerical results agree well with the measurements and also with accurate nonlinear numerical model runs by Ohyama & Nadaoka (1991), with the exception of some undulations in the transmitted waves. These undulations are caused by an error in modelling the bound wave. This error is inherent in MS-type models because the assumed vertical profile is for a free wave that is different in nature than the profile for a bound wave.

6. Summary and conclusions

The CMSE was shown to be in better agreement with exact linear theory compared with other MS-type equations (see Kim & Bai 2004). The main novel concept behind it is the use of a streamfunction formulation which allows the vertical profile assumption to accurately satisfy the kinematic bottom boundary condition.

In the present work, the CMSE was extended up to second order to enable nonlinear coupling between frequency components. This was done by applying Hamilton's principle to the IGN Lagrangian. The nonlinear CMSE exploits the same advantages of the linear CMSE also for nonlinear triad interactions, resulting in higher accuracy of the interactions between the waves and the bottom and an improved energy transfer between modes.

The model's validity is confirmed by comparison with an accurate numerical model and laboratory experiments over submerged obstacles and with an analytical perturbation solution of class III Bragg resonance. The results give good agreements, which reassure the use of the nonlinear CMSE for practical problems.

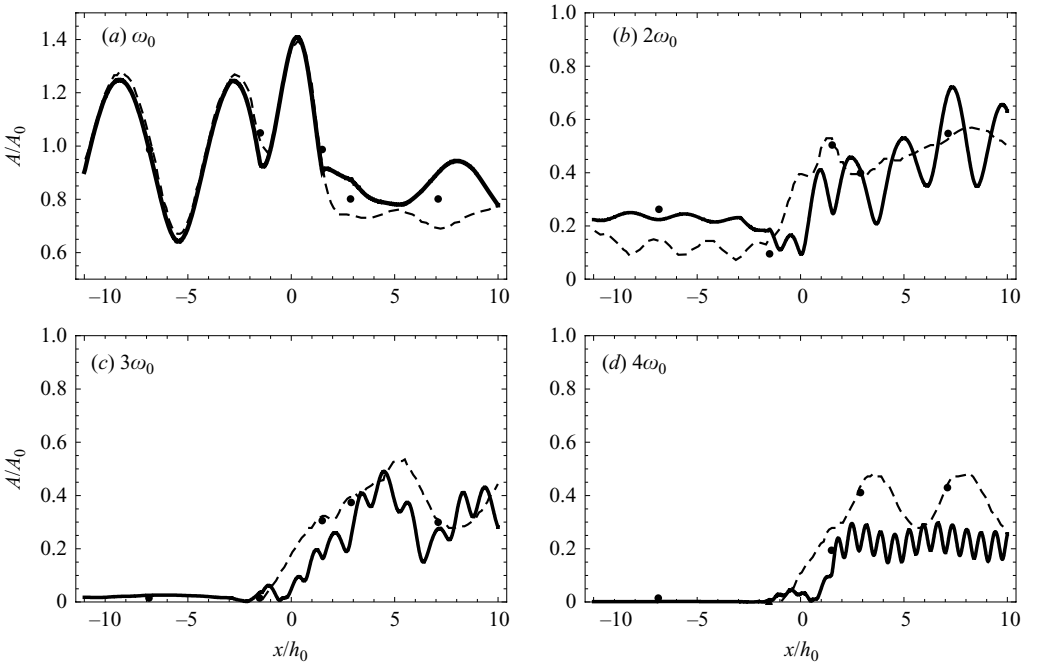

FIGURE 6. The numerical results of the nonlinear CMSE for the experiment of Ohyama *et al.* (1995) shown by the solid line. The dashed lines represent the fully nonlinear solution by Ohyama & Nadaoka (1991). The circles show the wave gauge measurements of the wave tank experiment. The wave amplitude is normalized by the first-harmonic incident wave amplitude, and the position is normalized by the flat bottom depth. Panels (*a*), (*b*), (*c*) and (*d*) indicate the first, second, third and fourth harmonics respectively.

This model is elliptic in nature and allows for solving problems that include reflection and refraction, as in harbour design. It is especially economic for narrow-banded wave spectra, as the number of triad interactions is relatively small. For broad-banded waves, the high-order Boussinesq models may be more economic, even though they need to be integrated in the time domain as well.

This research was supported by the US-Israel Binational Science Foundation (grant 2004-205) and by the Germany–Israel (BMBF-MOST) Joint Research programme (grant 1946).

REFERENCES

AGNON, Y., PELINOVSKY, E. & SHEREMET, A. 1998 Disintegration of cnoidal waves over smooth topography. *Stud. Appl. Math.* **101** (1), 49–71.

AGNON, Y. & SHEREMET, A. 1997 Stochastic nonlinear shoaling of directional. *J. Fluid Mech.* **345**, 79–99.

AGNON, Y., SHEREMET, A., GONSALVES, J. & STIASSNIE, M. 1993 Nonlinear evolution of a unidirectional shoaling wave field. *Coastal Engng* **20**, 29–58.

BEJI, S. & BATTJES, J. A. 1993 Experimental investigation of wave propagation over a bar. *Coastal Engng* **19**, 151–162.

DINGEMANS, M. W. 1994 Comparison of computations with Boussinesq-like models and laboratory measurements. *Tech Rep.* h1684.12. Delft Hydraulics.

Eldeberky, Y. & Madsen, P. A. 1999 Deterministic and stochastic evolution equations for fully dispersive and weakly nonlinear waves. *Coastal Engng* **38** (1), 1–24.

Ertekin, R. C. & Becker, J. M. 1998 Nonlinear diffraction of waves by a submerged shelf in shallow water. *J. Offshore Mech. Arctic Engng* **120** (4), 212–220.

Green, A. E. & Naghdi, P. M. 1976 Oblique wave incidence on a plane beach: the classical problem revisited. *Proc. R. Soc. Lond.* A **347**, 447–473.

Kaihatu, J. M. & Kirby, J. T. 1995 Nonlinear transformation of waves in finite water depth. *Phys. Fluids* **8**, 175–188.

Kim, J. W. & Bai, K. J. 2004 A new complementary mild-slope equation. *J. Fluid Mech.* **511**, 25–40.

Kim, J. W., Bai, K. J., Ertekin, R. C. & Wbster, W. C. 2001 A derivation of the Green–Naghdi equations for irrotational flows. *J. Engng Math.* **40**, 17–42.

Kim, J. W., Bai, K. J., Ertekin, R. C. & Wbster, W. C. 2003 A strongly nonlinear model for water waves in water of variable depth – the irrotational Green–Naghdi model. *J. Offshore Mech. Arctic Engng* **125**, 25–32.

Kim, J. W., Ertekin, R. C. & Bai, K. J. 2007 Linear and nonlinear wave models based on Hamilton's principle and stream-funcion theory: CMSE and IGN. In *ASME 2007 26th International Conference on Offshore Mechanics and Arctic Engineering*, 10–15 June 2007, San Diego, CA.

Liu, Y. & Yue, D. K. P. 1998 On generalized Bragg scattering of surface waves by bottom ripples. *J. Fluid Mech.* **356**, 297–326.

Luth, H. R., Klopman, G. & Kitou, N. 1980 Kinematics of waves breaking partially on an offshore bar; ldv measurements for waves with and without a net onshore current. *Tech Rep.* h1573. Delft Hydraulics.

Madsen, P. A., Fuhrman, D. R. & Wang, B. 2006 A Boussinesq-type method for fully nonlinear waves interacting with a rapidly varying bathymetry. *Coastal Engng* **53**, 487–504.

Mei, C. C. 1985 Resonant reflection of surface water waves by periodic sandbars. *J. Fluid Mech.* **152**, 315–335.

Ohyama, T., Kioka, W. & Tada, A. 1995 Applicability of numerical models to nonlinear dispersive waves. *Coastal Engng* **24**, 297–313.

Ohyama, T. & Nadaoka, K. 1991 Development of a numerical wave tank for analysis of nonlinear and irregular wave field. *Fluid Dyn. Res.* **8**, 23l–251.

Stiassnie, M. & Drimer, N. 2006 Prediction of long forcing waves for harbour agitation studies. *J. Waterway Port Coastal Ocean Engng* **132** (3), 166–171.

Toledo, Y. 2008 Refraction and diffraction of linear and nonlinear waves. PhD thesis, Technion–Israel Institute of Technology, Haifa, Israel.